polysaccharides

MDPI

Article

Okra Biomass-Derived Pectin-Rich Polysaccharide Composite Coating for Formulation-Dependent Surface Friction on Mango Fruit

Pikulthong Chaimongkol [1], Titita Bunyarit [2,3], Kingnapha Taosri [2,3], Sureerat Thomya [2,3], Bow Tinpovong [4], Nuttinee Salee [4], Aekarin Inpramoon [4], Ratchadaporn Jaimun [5], Nuttarut Pananda [6] and Malaiporn Wongkaew [4,*]

1 Program in General Education, Interdisciplinary and Technological College, Rajamangala University of Technology Lanna, Chiang Mai 50220, Thailand; c.pikulthong@rmutl.ac.th
2 Plant Bioactive Compound Laboratory, Faculty of Agriculture, Chiang Mai University, Chiang Mai 50200, Thailand; titita_bun@cmu.ac.th (T.B.); 690851008@cmu.ac.th (K.T.); sureerat_tho@cmu.ac.th (S.T.)
3 Postharvest Technology Research Center, Faculty of Agriculture, Chiang Mai University, Chiang Mai 50200, Thailand
4 Program in Food Production and Innovation, Interdisciplinary and Technological College, Rajamangala University of Technology Lanna, Chiang Mai 50220, Thailand; bowtinpovong@rmutl.ac.th (B.T.); nattinee@rmutl.ac.th (N.S.); aeengineer@rmutl.ac.th (A.I.)
5 Faculty of Arts and Architecture, Rajamangala University of Technology Lanna, Chiang Mai 50300, Thailand; ratchadaporn.jaimun@gmail.com
6 Program in Mechanical Engineering, Faculty of Engineering, Rajamangala University of Technology Lanna, Chiang Mai 50300, Thailand; nuttarut@rmutl.ac.th
* Correspondence: malaiporn@rmutl.ac.th

Abstract

Valorisation of agro-industrial biomass into functional coatings offers a sustainable approach to developing bio-based materials for postharvest applications. Although polysaccharide–lipid coatings are widely studied for their barrier properties, their effects on fruit–packaging friction remain poorly understood. This study recovered pectin-rich polysaccharides (OP) from okra-processing biomass and developed OP–beeswax (BW) composite coatings to modify mango–packaging friction and evaluate selected postharvest quality attributes. Conventional thermal extraction (CTE) and microwave-assisted extraction (MAE) yielded OP with comparable degrees of esterification but distinct hydration properties, with extraction yields of 4.28% and 5.47%, respectively ($p > 0.05$). The recovered OP exhibited low-methoxyl characteristics, with a degree of esterification of approximately 47%. Film optical and microstructural properties varied with OP and BW levels. Coating performance was evaluated on three independent mango fruits per treatment (n = 3; 21 fruits in total), with the same fruits used for friction and all quality measurements. Static and kinetic coefficients of friction (COFs) at the mango–corrugated plastic board interface were in the ranges of 0.45–0.59 and 0.42–0.58, respectively, demonstrating formulation-dependent frictional behaviour. T3 (1.0% OP + 1.0% BW) exhibited static and kinetic COFs of 0.46 and 0.42, respectively, comparable to the uncoated control (0.46 and 0.45), whereas T4 (2.0% OP + 1.0% BW) showed the highest values (0.59 and 0.58). After three days of storage, coating treatments significantly affected weight loss, firmness, and titratable acidity (TA), with the lowest weight loss observed in T6 (3.25%) and the highest TA in T2 (0.47%), whereas total soluble solids and pH did not differ among treatments. These findings demonstrate the potential of okra-processing biomass for developing bio-based coatings with tunable fruit–packaging friction, although their effectiveness in reducing transportation-induced damage requires further investigation.

Check for updates

Academic Editor: Waldo M. Argüelles-Monal

Received: 12 September 2026
Revised: 24 October 2026
Accepted: 30 October 2026
Published: 4 November 2026

Copyright: © 2026 by the authors. Licensee MDPI, Basel, Switzerland. This article is an open access article distributed under the terms and conditions of the Creative Commons Attribution (CC BY) license.

Keywords: biomass valorisation; coefficient of friction; circular economy; food waste; postharvest quality

1. Introduction

The transportation of fresh agricultural produce presents a major postharvest challenge, as vibration and mechanical shocks during handling and transit can cause bruising and other forms of mechanical damage. Meanwhile, growing demand for sustainable materials has encouraged the valorisation of agro-industrial biomass as a renewable source of functional biopolymers. Polysaccharides are particularly promising for biodegradable films and coatings because of their film-forming ability, biocompatibility, and biodegradability [1]. Polysaccharide-based coatings can form semipermeable barriers that limit moisture loss and gas exchange, helping maintain fruit quality during postharvest storage [2,3]. Among these, pectin is widely investigated for its film-forming and gas-barrier properties, although its hydrophilic nature can limit moisture resistance and surface functionality [3]. Incorporating hydrophobic components, such as beeswax (BW), into polysaccharide matrices can improve moisture-barrier properties and modify coating surface characteristics [4,5]. Beyond barrier performance, coating composition may influence the coefficient of friction (COF) between fruit surfaces and contacting materials. A lower COF may facilitate sliding and reduce tangential resistance, whereas a higher COF may restrict relative movement and improve fruit stability within packaging. However, the potential mechanical benefits depend on contact conditions, packaging configuration, and applied forces. Although polysaccharide–lipid coatings have been extensively studied for postharvest preservation, their effects on fruit-surface friction remain less explored. Understanding these formulation-dependent frictional properties may provide a foundation for future investigations into coating performance under transportation-related vibration and impact conditions.

Okra (*Abelmoschus esculentus* (L.) Moench) is a promising renewable source of pectin-rich polysaccharides, particularly rhamnogalacturonan-I (RG-I), whose branched structure contributes to distinctive rheological and functional properties [6,7]. Okra-derived polysaccharides exhibit favourable hydration, viscosity, film-forming, and biodegradable characteristics, supporting their potential application in edible films and coatings [8]. Their hydroxyl and carboxyl groups facilitate interactions with other polymers and lipid components, enabling the development of composite coatings with tailored barrier, mechanical, and surface properties [9]. Previous studies have demonstrated their potential for maintaining the postharvest quality of fresh produce [9–11], while recovery from okra-processing biomass offers an opportunity for sustainable biomass valorisation. Despite these advantages, research on polysaccharide-based fruit coatings has primarily focused on moisture retention, gas exchange, and postharvest quality, with limited attention to the relationships among coating composition, film properties, and fruit-surface friction. In particular, the influence of hydrophilic polysaccharide–hydrophobic lipid interactions on the coefficient of friction (COF) remains insufficiently understood. Investigating these relationships may provide insights into the development of bio-based coatings with tailored surface properties and their potential applications in postharvest handling and transportation.

To address this knowledge gap, this study aimed to valorise okra-processing biomass by recovering an okra pectin-rich polysaccharide (OP) for the development of sustainable OP–BW composite coatings. The effects of OP and BW concentrations on film characteristics, the frictional behaviour of coated mango fruit against a corrugated plastic board, and postharvest quality were investigated to elucidate formulation–property–function relationships. The potential relevance of friction modification to postharvest handling

and transportation is considered as a prospective application; however, fruit–fruit friction, vibration, impact, and bruising were not evaluated in the present study. These findings provide a basis for further application of the developed coatings to regulate fruit–fruit interactions and mitigate mechanical damage during transportation.

2. Materials and Methods

2.1. Materials

2.1.1. Okra-Processing Biomass

Frozen okra biomass was obtained from Union Fresh (2003) Co., Ltd., Chiang Mai, Thailand. The biomass consisted of off-grade okra generated during frozen processing, including pods with irregular sizes and cold-injury defects. The okra had an average width and length of 17.11 ± 1.91 and 34.74 ± 3.49 mm, respectively. The CIE L*a*b* colour values were L* = 33.88 ± 10.60, a* = −9.35 ± 1.58, and b* = 19.76 ± 4.24 (Figure 1). The moisture content was 93.86 ± 1.09% (wet basis).



Figure 1. Frozen okra biomass used as the raw material for OP extraction.

2.1.2. Mango Fruit

Ripe Chok Anan mangoes were obtained from Muang Mai Market, Muang, Chiang Mai, Thailand. Fruits were selected based on a specific gravity ranging from 1.01 to 1.02, as previously described by Wongkaew et al. [12] (Figure 2).

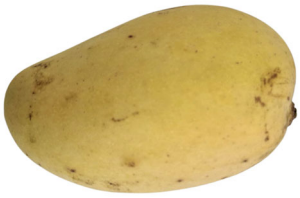


Figure 2. Chok Anan mango.

2.1.3. Chemicals and Reagents

Chemicals used for the analysis of OP characteristics were supplied by Sigma-Aldrich (St. Louis, MO, USA), RCI Labscan Limited (Bangkok, Thailand), and AppliChem GmbH, an ITW Company (Darmstadt, Germany).

2.2. Recovery and Characterisation of Okra Pectin-Rich Polysaccharide

2.2.1. OP Extraction

Frozen okra biomass obtained from Union Fresh (2003) Co., Ltd., Chiang Mai, Thailand, was dried in a hot-air oven at 70 °C until a constant weight was reached and the moisture content was below 5% (dry basis). The dried material was ground and passed through a 60-mesh sieve to obtain a uniform powder prior to extraction. OP was extracted using two different heating techniques: conventional extraction (CTE) and microwave-assisted extraction (MAE). For each extraction, 10 g of the dried okra powder was dispersed in

200 mL of distilled water. For CTE, the mixture was heated at 90 °C for 30 min using a conventional heating system. For MAE, the mixture was treated using a phase-controlled microwave system operated at 900 W while maintaining the extraction temperature at 90 °C for 30 min (adapted from [13]). After extraction, each mixture was filtered, and the resulting filtrate was separately mixed with two volumes of cold 95% (*v*/*v*) ethanol to induce OP precipitation. The precipitated OP was recovered and dried in a hot-air oven at 40 °C to a constant weight [14].

2.2.2. Extraction Yield and Physicochemical Properties

- Yield Percentage

The OP yield (%) was determined according to Equation (1).

$$\text{Yield } (\%) = \frac{M_0}{M} \times 100 \quad (1)$$

Here, M_0 (g) = the weight of dried OP, and M (g) = the weight of dried okra powder.

- CIE Colour

Colour measurements were performed using the CIE L*a*b* colour space with a ColorFlex EZ 45/0 LAV colourimeter (HunterLab, Reston, VA, USA). In this system, L* represents lightness, ranging from 0 (black) to 100 (white); a* indicates the red–green axis, with positive values corresponding to redness and negative values to greenness; and b* represents the yellow–blue axis, with positive values indicating yellowness and negative values indicating blueness [12].

- Moisture Content and Water Activity

Moisture content was determined using an OHAUS MB25 moisture analyser (OHAUS Corporation, Parsippany, NJ, USA), while water activity (a_w) was measured using a Freund EZ-200 water activity meter (Freund Corporation, Tokyo, Japan).

2.2.3. Chemical and Structural Characterisation

- Equivalent Weight (Eq.W.)

The Eq.W. was determined according to the method of Girma and Worku [15] and Virk and Sogi [16]. Briefly, 0.5 g of OP was weighed into a 250 mL conical flask and moistened with 5 mL of ethanol. Subsequently, 1.0 g of NaCl and 100 mL of deionised water (DIH_2O) were added, followed by three drops of phenol red indicator. The solution was titrated with 0.1 N NaOH until a stable pink endpoint (pH 7.5) was reached, with the colour persisting for at least 30 s. The equivalent weight was calculated using Equation (2).

$$\text{Eq.W.}(\text{g/mol}) = \frac{1000 \times \text{Weight of sample}(\text{g})}{\text{Concentration of NaOH}(\text{N}) \times \text{Volume of NaOH}(\text{mL})} \quad (2)$$

- Methoxyl Content (Mox)

The Mox was determined according to the method of Girma and Worku [15] and Virk and Sogi [16]. OP (0.5 g) was weighed, and 25 mL of 0.25 N NaOH was added. The mixture was stirred and allowed to stand at room temperature for 30 min. Subsequently, 25 mL of 0.25 N HCl was added, and the mixture was titrated against 0.1 N NaOH to the same endpoint as previously described [16]. Methoxyl content was calculated using Equation (3).

$$\text{Mox } (\%) = \frac{3.1 \times \text{Concentration of NaOH } (\text{N}) \times \text{Volume of NaOH } (\text{mL})}{\text{Weight of sample } (\text{g})} \quad (3)$$

- Total Anhydrouronic Acid Content (AUA)

The AUA content was determined according to the method of Virk and Sogi [16]. AUA is a crucial parameter for evaluating the purity, degree of esterification, and physicochemical properties of OP. The AUA content was calculated using the equivalent weight and methoxyl content according to Equation (4).

$$\text{AUA } (\%) = \frac{176 \times \text{Concentration of NaOH}(\text{ N}) \times (\text{A} + \text{B}) \times 100}{\text{Weight of sample } (\text{g}) \times 1000} \quad (4)$$

Here, the molecular unit of AUA (1 unit) = 176 g;
A = mL (titrated) of NaOH from equivalent weight determination;
B = mL (titrated) of NaOH from methoxyl content determination.

- Degree of Esterification (DE)

The DE of the extracted OP was determined according to the method of Virk and Sogi [16] using the methoxyl and AUA contents. The DE was calculated using Equation (5).

$$\text{DE } (\%) = \frac{176 \times \%\text{Mox}}{31 \times \%\text{AUA}} \times 100 \quad (5)$$

- FTIR Analysis and Degree of Esterification (FTIRDE)

Fourier-transform infrared spectroscopy (FTIR) was used to analyse the chemical structure of the extracted OP using an FTIR spectrometer (PerkinElmer, Shelton, CT, USA). The FTIR spectra were recorded over a wavenumber range of 4000–400 cm^{-1} at a spectral resolution of 4 cm^{-1} with 32 scans per spectrum. Baseline correction of the FTIR spectra was performed using Microsoft Excel 2021 by applying a linear two-point baseline between approximately 1800 and 1500 cm^{-1}, spanning both carbonyl bands, without spectral normalisation. Measurements were performed in triplicate (n = 3), and the degree of esterification (DE) was calculated separately for each replicate according to Wang et al. [17] using Equation (6):

$$\text{FTIRDE } (\%) = \frac{A_{1745}}{A_{1745} + A_{1630}} \times 100 \quad (6)$$

where A_{1745} and A_{1630} represent the absorbance intensities (peak heights) at approximately 1745 and 1630 cm^{-1}, corresponding to methyl-esterified and non-methyl-esterified carboxyl groups, respectively.

2.2.4. Functional Properties

- Water Absorption Capacity (WAC)

The WAC was determined according to the method described by Beuchat [18], with slight modifications. Briefly, 1 g of the sample (W_0) was dispersed in 10 mL of distilled water, vortexed thoroughly, and allowed to equilibrate for 15 min. The mixture was then centrifuged at 1000× *g* for 10 min, after which the supernatant was carefully discarded. The tubes were inverted to drain any residual water, and the weight of the hydrated sample (W_2) was recorded. WAC was subsequently calculated using Equation (7).

$$\text{WAC } (\text{g}/\,g_{sample}) = \left(\frac{W_2 - W_0}{W_0}\right) \quad (7)$$

Here, W_0 is the initial dry sample weight (g), and W_2 is the weight of the hydrated sample after centrifugation and removal of the supernatant (g).

- Water Solubility Index (WSI) and Swelling Power (SP)

The WSI and SP of the extracted okra pectin-rich polysaccharide powder (OP) were evaluated following the method of Kaur and Singh [19], with minor modifications. A 1 g

portion of the powder (W_0) was accurately weighed into a pre-weighed centrifuge tube. Subsequently, 20 mL of distilled water was added. The suspension was thoroughly mixed and incubated in a water bath at 90 °C for 10 min to facilitate hydration and swelling. Following heat treatment, the suspension was allowed to cool to room temperature for 15 min before centrifugation at 3000× *g* for 10 min to separate the soluble fraction from the hydrated sediment. The supernatant was carefully transferred into a pre-weighed crucible and dried at 100 °C for 24 h until the soluble solids were completely recovered. The weight of the dried soluble fraction was recorded as W_2. Meanwhile, the hydrated sediment retained in the centrifuge tube was weighed and recorded as W_3. The WSI and SP were subsequently determined using the following equations:

$$\mathrm{WSI}\left(\mathrm{g}/100\ g_{sample}\right) = \frac{W_2}{W_0} \times 100 \quad (8)$$

$$\mathrm{SP}\ \left(\mathrm{g}/\ g_{sample}\right) = \frac{W_3}{W_0 - W_2} \quad (9)$$

2.3. Development of Bio-Based Composite Coating

2.3.1. Experimental Design and Film Formulations

OP obtained by MAE was used for coating formulation development. This choice was made primarily because MAE-derived OP had a significantly lower water solubility index (WSI), which was considered potentially advantageous for a coating intended to remain on the fruit surface under humid storage conditions, together with a numerically (but not significantly) higher extraction yield. The two extracts did not differ significantly in methoxyl content or degree of esterification, indicating that both were low-methoxyl pectin-rich fractions. However, MAE-derived OP also had a lower anhydrouronic acid (AUA) content and higher water activity, and its higher water absorption capacity may increase moisture sensitivity. MAE-derived OP was therefore selected as a practical choice for formulation development rather than as an extract with demonstrated overall superiority, and coatings prepared from CTE-derived OP were not evaluated. Based on preliminary studies, the coating formulations were developed by varying the concentrations of OP, carboxymethyl cellulose (CMC), beeswax (BW), and titanium dioxide (TiO_2). The concentrations of CMC and TiO_2 were fixed at 0.5% (*w*/*v*) and 0.01% (*w*/*v*), respectively, based on their favourable performance in preliminary film formation tests. The formulation optimisation was subsequently conducted using a 2 × 2 factorial experiment arranged in a completely randomised design (CRD). The independent variables were the levels of OP and BW, as presented in Table 1. Additionally, each treatment was compared with a control formulation without OP (CTRL-No OP) and a control formulation without BW (CTRL-No BW).

Table 1. Composition of the OP–BW coating formulations (T1–T4 factorial core) and control treatments (T5–T7).

Treatment Group	Treatment	OP (% *w*/*v*)	BW (% *w*/*v*)	CMC (% *w*/*v*)	TiO_2 (% *w*/*v*)	Tween 80 (% *w*/*v*)	PEG 400 (% *w*/*v*)
Factorial core	T1	1.0	0.5	0.5	0.01	0.3	30% of total polymer weight
	T2	2.0	0.5	0.5	0.01	0.3	
	T3	1.0	1.0	0.5	0.01	0.3	
	T4	2.0	1.0	0.5	0.01	0.3	
Control	T5 (CTRL-No OP)	0.0	1.0	0.5	0.01	0.3	
	T6 (CTRL-No BW)	2.0	0.0	0.5	0.01	0.3	
	T7 (No coating)	-	-	-	-	-	-

2.3.2. Coating Preparation

The preparation procedure of the coating formulations was adapted from the methods of Chaichi et al. [20] and Chao et al. [21]. OP was dissolved in distilled water at 70–80 °C under magnetic stirring until completely dissolved. CMC was then added and dispersed by homogenisation at 5000 rpm for 5 min. The resulting dispersion was then incorporated into the OP solution, followed by the addition of polyethylene glycol 400 (PEG 400) at 30% (*w*/*w*) of the total polymer content as a plasticiser. The mixture was further stirred for 10 min to ensure homogeneity. Beeswax, at the levels specified in Table 1, was melted at 75–80 °C. Tween 80 (0.30%, *w*/*v*) was dissolved in distilled water and heated to the same temperature. The molten beeswax was gradually added to the Tween 80 solution and homogenised at 5000 rpm for 3–5 min to obtain a stable and uniform emulsion. Food-grade TiO_2, at the concentration shown in Table 1, was dispersed in a small volume of distilled water and homogenised for 10 min to minimise particle aggregation. Subsequently, the TiO_2 suspension and beeswax emulsion were sequentially incorporated into the OP–CMC solution. The final mixture was homogenised at 5000 rpm for 5 min using a high-speed homogeniser (Ultra-Turrax T-25 (IKA®-Werke GmbH & Co. KG, Staufen, Germany)), and the final volume of each treatment was adjusted to 1000 mL with distilled water. No additional degassing step was performed prior to film casting or coating application. For film preparation, 50 mL of each film-forming mixture was poured into a glass Petri dish (15 cm diameter; casting area ≈ 177 cm^2) and dried in a hot-air oven at 40 °C for 24 h. Three independent film batches were prepared for each formulation using separately prepared film-forming mixtures (n = 3). After drying, the films were carefully peeled from the Petri dishes and conditioned at 25 ± 2 °C and 60 ± 5% relative humidity for 24 h prior to characterisation. The developed films were subsequently characterised for their thickness, optical, and microstructural properties. Throughout this study, "films" refers to free-standing films cast from the formulations in Petri dishes and used as model systems for characterising the intrinsic optical, thickness, and microstructural properties of each formulation, whereas "coatings" refers to the layers formed on the mango peel by immersion (Section 2.5.1). Because the casting volume, substrate, drying conditions, and geometry differed from those of fruit coating, film properties were not assumed to represent the thickness, continuity, or microstructure of the coatings on fruit.

2.4. Characterisation of Bio-Based Films

2.4.1. Optical Properties of Composite Films

- Colour

Colour analysis was performed using a calibrated colorimeter according to the CIE L*a*b* colour space. The colour parameters L* (lightness), a* (redness/greenness), and b* (yellowness/blueness) were recorded. The whiteness index (WI) was calculated using Equation (10) [22].

$$WI = 100 - \sqrt{(100 - L)^2 + a^2 + b^2} \quad (10)$$

- Optical Properties

Film transparency was evaluated using a UV–Vis spectrophotometer (SpectraMax iD3, Molecular Devices, San Jose, CA, USA). Film specimens were placed in quartz cuvettes, and their absorbance was measured at 600 nm. Film opacity was subsequently calculated according to Equation (11) [23].

$$\text{Opacity} = \frac{A_{600}}{d} \quad (11)$$

Here, A_{600} represents the absorbance measured at 600 nm, and d denotes the average film thickness expressed in millimetres.

2.4.2. Film Thickness

The film thickness was measured using a modified method [24]. Film thickness was measured using a digital micrometre (Precision Measuring, Xi'an, China) with an accuracy of 0.01 mm. Measurements were taken at five randomly selected positions across each film (casting area $\approx$ 177 cm^2), avoiding the film edges, and the mean value was calculated to represent the thickness of each independently prepared film. The reported thickness was expressed as the mean $\pm$ standard deviation of three independent film batches (n = 3).

2.4.3. Film Microstructure

The microstructure of the films was characterised using scanning electron microscopy (SEM). Samples were mounted onto specimen stubs using double-sided adhesive tape and sputter-coated with gold to ensure conductivity. Imaging was performed using an SEM (JEOL JCM-7000, Tokyo, Japan) at an accelerating voltage of 15 kV and a magnification of $\times$500 and $\times$2000 [13]. For each formulation, one independently prepared film was examined, with three randomly selected fields observed per film at each magnification. As only one film per formulation was examined, SEM observations were used solely for qualitative morphological assessment and were not subjected to statistical analysis. Accordingly, the SEM images are presented as representative observations of film surface and cross-sectional morphology, and no conclusions regarding statistically significant differences between formulations were drawn from these observations.

2.5. Application of Composite Coatings on Mango Fruit

2.5.1. Mango Coating Treatment

A total of 21 ripe Chok Anan mangoes of uniform size and maturity (specific gravity 1.01–1.02) and free from visible defects were obtained from a single purchase lot at Muang Mai Market in July 2026. The fruits were numbered individually and randomly assigned to seven treatments (T1–T7; three fruits per treatment) using a random number table. For each coating formulation, three independent batches of film-forming mixture were prepared on the same day. Each batch was applied to one fruit by immersion for 1 min, followed by draining for 5 min. Each fruit was therefore an independent experimental unit (n = 3 per treatment). Control fruits (T7) were left untreated. All fruits were then dried under cool air at 25 $\pm$ 2 °C and 60 $\pm$ 5% relative humidity for 24 h until touch-dry. The end of this drying period was designated Day 0. On Day 0, static and kinetic coefficients of friction (COFs) and initial fruit weight were measured on all 21 fruits, including the uncoated controls, so that all treatments received the same handling before storage. Fruits were then stored at 25 $\pm$ 2 °C for 3 days. On Day 3, fruit weight and peel colour were measured non-destructively, followed by destructive firmness testing. TSS, pH, and TA were then determined on pulp taken from both cheeks of the same fruit, pooled, and homogenised. Coating pickup (mass of coating retained per unit fruit surface area) and coating thickness on the fruit surface were not measured. The amount of coating deposited may therefore have differed between formulations, for example because of differences in viscosity, and this may have contributed to the observed differences in COF and quality.

2.5.2. Surface Friction Measurement

The static and kinetic coefficients of friction (COFs) of coated and uncoated mango fruit were determined on Day 0, immediately following the 24 h drying period described in Section 2.5.1, using an inclined-plane method adapted from Kelemenová et al. [25]. The counter-surface was a white corrugated polypropylene board (5.00 mm), representative of reusable fruit-packaging crates, mounted on the inclined plane with its smooth outer face upward and its flutes oriented parallel to the sliding direction. The same board was used for

all treatments. Before each fruit was tested, the contact area was wiped with a dry lint-free cloth and allowed to dry for at least 1 min, and the board was visually inspected after each trial for residue transfer. Trials showing visible transfer were discarded and repeated after cleaning. To avoid systematic bias from progressive board wear, fruits were tested in a randomised order across treatments. Each fruit was placed at a marked starting position with its cheek in contact with the board and its long axis parallel to the sliding direction to minimise rolling. The plane was inclined from 0° at 1.0° s^{-1}, and the angle was monitored with a calibrated digital inclinometer. Inclination was stopped immediately at the onset of sliding, and this critical angle was held constant while the fruit slid along the plane. The static COF was calculated using Equation (12). Fruit motion was recorded at 30 frames s^{-1}, and the sliding time (Δt) was determined from the first frame showing fruit displacement to the frame at which the fruit reached the end of the sliding distance (L_p = 0.8 m). Assuming motion from rest with constant acceleration, the kinetic COF was calculated at the same inclination angle (α) using Equation (13). As both COFs represent the ratio of frictional force to normal force (mg cos α), fruit mass cancels out in the calculations, making the COFs independent of fruit mass (278.0–367.0 g). Three sliding trials were performed per fruit, with the fruit returned to the starting position and allowed to rest for 30 s between trials. The three measurements were averaged to obtain one value per fruit (n = 3 fruits per treatment). Trials showing visible rolling or rotation were discarded and repeated.

$$f_s = \tan \alpha \tag{12}$$

$$f_k = \tan \alpha - \frac{2L_p}{g \times \Delta t^2 \times \cos \alpha} \tag{13}$$

Here, α is the inclination angle at which the mango fruit begins to slide, L_p is the sliding distance of the mango fruit (m), g is the gravitational acceleration (9.81 m/s^2), and Δt is the time required for the fruit to travel the sliding distance (s).

2.5.3. Mango Fruit Quality Assessment

- Weight Loss (%)

Each mango fruit was weighed on Days 0 and 3 of storage using an electronic balance (TANITA KD-321, Tanita Corporation, Itabashi, Tokyo, Japan) with a precision of ±0.1 g. Percentage weight loss was calculated relative to the initial weight of each fruit [26].

- Colour and Firmness

Mango peel colour was measured using a portable colourimeter (NH3, Guangdong Threenh Technology Co., Ltd., Zengcheng, Guangzhou, China) and expressed according to the CIE L*a*b* colour system. The L* value represents lightness (0 = black and 100 = white), while a* represents the green (−) to red (+) axis and b* represents the blue (−) to yellow (+) axis. Six replicate measurements were taken for each fruit. Fruit firmness was determined using a fruit penetrometer (QA version FT-02, QA Supplies LLC, Norfolk, VA, USA), with six replicate measurements taken from each fruit. Firmness was measured on Day 3 only, on the same fruits used for colour and weight-loss determinations, at six positions around the equatorial region (three per cheek) after removal of a small peel disc.

- Chemical Analysis

The total soluble solids (TSS) content of mango pulp was measured using a digital refractometer and expressed as °Brix. The pH was determined using a calibrated pH meter. TA was determined by acid–base titration [27]. Mango pulp (2.00 g) was homogenised with 23 mL of distilled water and filtered. The entire filtrate was titrated with standardised 0.1 N NaOH to pH 8.2, monitored with a calibrated pH meter, using phenolphthalein as

the indicator. Because the entire filtrate was titrated, no dilution factor was applied. TA was expressed as g citric acid per 100 g fresh pulp using Equation (14):

$$\text{TA } (\%) = \frac{\mathbf{V} \times \mathbf{N} \times \mathbf{0.064} \times \mathbf{100}}{\text{m}} \quad (14)$$

where V is the volume of NaOH consumed (mL), N is the normality of NaOH (eq/L), 0.064 is the milliequivalent weight of anhydrous citric acid (g.m/Eq), and m is the mass of fresh mango pulp (g).

2.6. Statistical Analyses

The experimental units comprised independent extraction runs for OP characterisation (n = 3 per extraction method), independently prepared film batches for film properties (n = 3 per formulation), and individual mango fruits for COF and fruit quality measurements (n = 3 per treatment, with one fruit per independent coating batch; Section 2.5.1). Repeated measurements within each experimental unit were treated as subsamples and averaged before statistical analysis, including five thickness measurements per film, three sliding trials per fruit for COF determination, six peel-colour measurements per fruit, and six firmness measurements per fruit. Differences between CTE and MAE were evaluated using one-way analysis of variance (ANOVA) with two levels, equivalent to an independent-samples *t*-test; therefore, no post hoc comparisons were required. For film properties and fruit characteristics, differences among the seven treatments (T1–T7) were assessed using one-way ANOVA followed by Tukey's honestly significant difference (HSD) test ($p < 0.05$). For the 2 × 2 factorial design comprising T1–T4, two-way ANOVA was performed to evaluate the main effects of OP and BW concentrations and their interaction (OP × BW). The control treatments (T5–T7) were excluded from the factorial analysis. Given the limited statistical power associated with the small sample size (n = 3), descriptive statistics were reported as means ± standard deviations (SDs). Effect sizes were expressed as partial eta-squared (η^2) for the factorial ANOVA. All statistical analyses were performed using IBM SPSS Statistics version 27.0.1 (IBM Corp., Armonk, NY, USA). Principal component analysis (PCA) was performed as an exploratory analysis using XLSTAT version 2026.1.2 (Addinsoft, Paris, France) on four variables (static COF, kinetic COF, weight loss, and TA), with each fruit as an observation (21 observations; n = 3 per treatment). Since the variables were measured on different scales, PCA was based on the Pearson correlation matrix; that is, all variables were mean-centred and scaled to unit variance before analysis. As static and kinetic COF were strongly correlated, a sensitivity analysis was performed using static COF only. PCA results are presented in the Supplementary Materials (Figure S1 and Table S2).

3. Results and Discussion

3.1. Characteristics of Okra Biomass-Derived Pectin-Rich Polysaccharide

3.1.1. Physicochemical and Functional Properties

Okra pectin-rich polysaccharides (OP) were extracted directly using conventional thermal extraction (CTE) and microwave-assisted extraction (MAE). The extraction method did not significantly affect yield ($p > 0.05$), although MAE produced a numerically higher yield (5.47 ± 0.88%) than CTE (4.28 ± 0.67%) (Table 2). Microwave heating can promote plant tissue disruption, solvent penetration, and mass transfer, potentially improving polysaccharide recovery [28–30]. Similarly, Fatima et al. [30] reported higher OP yields using MAE (15.29%) than CTE (11.72%). The lower yields observed in the present study may reflect differences in okra variety, raw material characteristics, and extraction conditions.

However, the numerical increase observed with MAE should not be interpreted as a statistically significant improvement in extraction efficiency.

Table 2. Physicochemical characteristics of OP extracted using conventional (CTE) and microwave-assisted extraction (MAE).

Characteristics	Extraction Methods	
	CTE	**MAE**
Yield (%) ^{ns}	4.28 ± 0.67	5.47 ± 0.88
Colour		
- L* *	75.34 ± 0.03	75.11 ± 0.01
- a* ^{ns}	0.67 ± 0.06	0.60 ± 0.03
- b* ^{ns}	10.94 ± 0.87	9.72 ± 0.48
Moisture content (% dry basis) ^{ns}	10.69 ± 0.14	10.08 ± 0.95
Water activity *	0.30 ± 0.03	0.39 ± 0.01
Functional properties		
- Water absorption capacity * (WAC; g/g dry sample)	8.29 ± 0.18	18.17 ± 0.17
- Water solubility index * (WSI; g/100 g dry sample)	14.61 ± 2.37	9.57 ± 1.34
- Swelling power ^{ns} (SP; g/g dry sample)	10.31 ± 1.68	12.07 ± 0.30
Chemical characteristics		
- Equivalent weight (Eq.W.; g/mol) *	1002.95 ± 20.33	1064.15 ± 22.65
- Methoxyl content (Mox; %) ^{ns}	2.74 ± 0.12	2.56 ± 0.40
- Total anhydrouronic acid content (AUA; %) *	33.10 ± 0.39	31.09 ± 0.54
- Degree of esterification (DE; %) ^{ns}	46.96 ± 1.66	46.79 ± 0.88

Data are expressed as mean ± standard deviation. * The differences were statistically significant ($p < 0.05$) as determined, while "^{ns}" indicates no significant difference by *t*-test analysis.

The extraction method had a statistically significant but negligible effect on the lightness (L*) of the recovered OP powders ($p < 0.05$), with values of 75.34 and 75.11 for CTE and MAE, respectively. In contrast, no significant differences were observed in a* and b* values ($p > 0.05$), indicating that microwave-assisted extraction did not cause noticeable discoloration under the conditions investigated [31,32]. Moisture content was also comparable between CTE (10.69 ± 0.14%) and MAE (10.08 ± 0.95%; $p > 0.05$), while water activity (a_w) ranged from approximately 0.30 to 0.39. These low a_w values indicate limited water availability for microbial growth, suggesting favourable storage stability when the powders are protected from moisture uptake through appropriate packaging and storage conditions [33,34].

The hydration properties of the recovered OP differed between extraction methods. MAE exhibited significantly higher water absorption capacity (WAC; 18.17 ± 0.17 g/g dry sample) than CTE (8.29 ± 0.18 g/g dry sample; $p < 0.05$), potentially reflecting differences in polysaccharide structure, composition, and interactions with water [35–37]. In contrast, the water solubility index (WSI) was significantly lower for MAE (9.57 ± 1.34 g/100 g dry sample) than for CTE (14.61 ± 2.37 g/100 g dry sample; $p < 0.05$). These contrasting responses suggest that MAE produced a polysaccharide fraction with greater water retention but a smaller soluble fraction, highlighting the distinct hydration mechanisms represented by WAC and WSI [38,39]. Swelling power (SP) did not differ significantly between CTE (10.31 ± 1.68 g/g dry sample) and MAE (12.07 ± 0.30 g/g dry sample; $p > 0.05$). MAE

enhanced water absorption capacity and reduced water solubility without significantly affecting swelling power, demonstrating that extraction conditions influence the hydration functionality of OP [19,40].

3.1.2. Physicochemical Characteristics

The chemical characteristics of the recovered OP varied between extraction methods (Table 2). MAE exhibited a significantly higher equivalent weight (Eq.W.; 1064.15 ± 22.65 g/mol) than CTE (1002.95 ± 20.33 g/mol), whereas methoxyl content (Mox) and degree of esterification (DE) did not differ significantly ($p > 0.05$). Both extracts exhibited low Mox contents (2.56–2.74%) and DE values below 50% (46.79–46.96%), indicating characteristics consistent with low-methoxyl pectin and suggesting potential for calcium-mediated gelation [41,42]. The anhydrouronic acid (AUA) content was significantly higher in CTE (33.10 ± 0.39%) than in MAE (31.09 ± 0.54%). However, the relatively low AUA contents of both extracts suggest substantial non-pectic constituents, potentially including neutral sugars, proteins, and minerals associated with okra mucilage [43]. Consequently, the recovered material is more appropriately described as a pectin-rich polysaccharide fraction rather than purified pectin [44]. MAE influenced Eq.W. and AUA content but did not significantly alter Mox or DE under the extraction conditions investigated. Neither extraction method was clearly superior. MAE yielded OP with lower water solubility and higher water absorption capacity, whereas CTE yielded OP with a higher AUA content and lower water activity; yield, swelling power, methoxyl content, and degree of esterification did not differ significantly. The choice between methods therefore depends on the intended application. For coating development, the lower solubility of MAE-derived OP was prioritised, as described in Section 2.3.1.

The FTIR spectra of pectin-rich polysaccharides extracted by CTE and MAE exhibited similar spectral profiles and absorbance intensities (Figure 3), suggesting that the extraction methods did not substantially alter the major functional groups of the recovered polysaccharides. Baseline correction was performed using Microsoft Excel 2021 by applying a linear two-point baseline between approximately 1800 and 1500 cm^{-1}, without spectral normalisation. However, comparisons of absorbance intensities should be interpreted cautiously because spectral normalisation was not applied. The characteristic carbohydrate fingerprint region (950–1200 cm^{-1}) showed absorption bands at 1022, 1106, and 1149 cm^{-1}, associated with C–C, C–O, and glycosidic C–O–C vibrations of the polysaccharide backbone [45–47]. Bands at 1045 and 1076 cm^{-1} may indicate contributions from neutral sugar residues, including arabinose, xylose, and galactose [48]. The esterified carbonyl band at approximately 1745 cm^{-1} and the ionised carboxylate band at 1590–1630 cm^{-1} were used to estimate the degree of esterification (DE). Both extracts exhibited DE values below 50% (CTE: 33.94 ± 1.15%; MAE: 35.39 ± 0.54%), as determined by FTIR spectroscopy, indicating characteristics consistent with low-methoxyl pectin [45,48]. These values were lower than those obtained by titration (approximately 47%), possibly due to differences in analytical principles and interference from non-pectic components affecting both FTIR absorption bands and titration measurements. Additional bands at 1540–1560 cm^{-1} may reflect residual protein amide groups, while C–H stretching at 2930–2980 cm^{-1} and broad O–H stretching at approximately 3200–3600 cm^{-1} indicate carbohydrate structures and hydrogen bonding [17]. The comparable FTIR profiles suggest that MAE preserved the principal functional groups of the recovered pectin-rich polysaccharides relative to CTE.

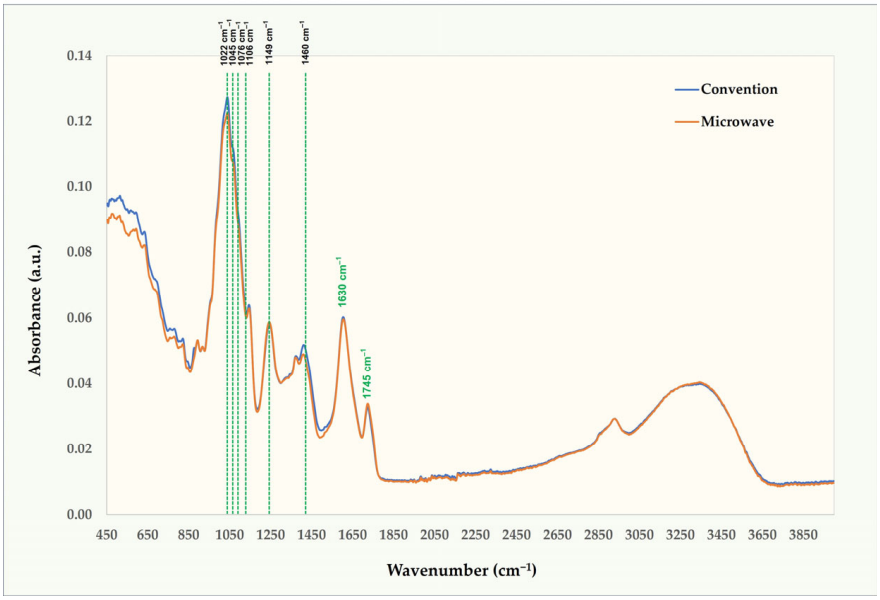


Figure 3. FTIR spectra of okra pectin (OP) extracted from okra biomass using conventional and microwave-assisted extraction methods, recorded over the wavenumber range of 4000–400 cm^{-1} at a spectral resolution of 4 cm^{-1} with 32 scans per spectrum. Measurements were performed in triplicate (n = 3) for each extraction method.

3.2. Surface and Microstructure of Bio-Based Films

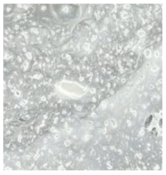
3.2.1. Surface Characteristics

The optical properties of the bio-based films varied significantly among formulations (Table 3). Lightness (L*) ranged from 56.87 to 87.31, with T5 (without OP) exhibiting the highest L* (87.31 ± 0.76) and lowest b* (4.65 ± 0.31), whereas T6 (without BW) showed the lowest L* (56.87 ± 1.53). OP-containing films exhibited higher a* and b* values, indicating a more pronounced yellow–brown appearance. Two-way ANOVA of T1–T4 revealed significant main effects of OP ($F = 10.370$, $p = 0.012$) and BW ($F = 15.314$, $p = 0.004$) on L*, without a significant interaction ($p = 0.091$; Table 4). In contrast, a* and b* were significantly affected by both factors and their interaction (all $p \leq 0.001$), with particularly strong OP × BW interactions for a* ($F = 44.870$) and b* ($F = 241.777$). These findings indicate that film colour depended on OP concentration and its interaction with BW, potentially reflecting the inherent pigments and residual compounds in the extracted polysaccharide fraction [49].

Table 3. Surface characteristics of different bio-based film formulations.

Properties	Bio-Based Film Formulations					
	T1	**T2**	**T3**	**T4**	**T5**	**T6**
Colour						
- L*	67.18 ± 2.15 ^{c}	65.28 ± 0.60 ^{c}	75.71 ± 3.94 ^{b}	68.20 ± 2.28 ^{c}	87.31 ± 0.76 ^{a}	56.87 ± 1.53 ^{d}
- a*	5.28 ± 0.11 ^{b}	5.98 ± 0.03 ^{b}	2.59 ± 0.26 ^{c}	5.87 ± 0.60 ^{b}	−1.07 ± 0.02 ^{d}	8.93 ± 0.70 ^{a}
- b*	21.11 ± 0.57 ^{c}	19.10 ± 0.44 ^{d}	17.30 ± 0.28 ^{e}	26.26 ± 0.95 ^{a}	4.65 ± 0.31 ^{f}	23.05 ± 0.93 ^{b}
Thickness (mm)	0.07 ± 0.01 ^{c}	0.09 ± 0.02 ^{b}	0.08 ± 0.01 ^{b}	0.09 ± 0.01 ^{b}	0.21 ± 0.06 ^{a}	0.03 ± 0.01 ^{d}
Opacity	5.98 ± 0.20 ^{b}	9.27 ± 0.66 ^{a}	7.30 ± 0.32 ^{b}	6.52 ± 0.86 ^{b}	3.31 ± 0.18 ^{c}	8.64 ± 0.86 ^{a}

Table 3. *Cont.*

Properties	Bio-Based Film Formulations					
	T1	**T2**	**T3**	**T4**	**T5**	**T6**
Whiteness index (WI)	60.60 ± 1.53 ^{c}	59.92 ± 0.53 ^{c}	70.01 ± 3.34 ^{b}	58.33 ± 2.18 ^{c}	86.44 ± 0.78 ^{a}	50.28 ± 1.66 ^{d}
						

Values are expressed as mean ± standard deviation (SD, n = 3). Different superscript letters within the same row indicate significant differences among the six formulations (Tukey's HSD test, $p < 0.05$). The formulations were as follows: T1 = 1.0% OP + 0.5% BW; T2 = 2.0% OP + 0.5% BW; T3 = 1.0% OP + 1.0% BW; T4 = 2.0% OP + 1.0% BW; T5 = CTRL–No OP; and T6 = CTRL–No BW.

Table 4. Effects of the main factors (OP and BW) on the optical properties of bio-based films (T1–T4).

Surface Characteristics	Effect	F	*p*-Value	Partial η^2
L*	OP	10.37	0.012	0.565
	BW	15.314	0.004	0.657
	OP × BW	3.68	0.091	0.315
a*	OP	106.517	0	0.93
	BW	52.859	0	0.869
	OP × BW	44.87	0	0.849
b*	OP	96.824	0	0.924
	BW	22.516	0.001	0.738
	OP × BW	241.777	0	0.968
Whiteness index	OP	24.718	0.001	0.755
	BW	9.894	0.014	0.553
	OP × BW	19.601	0.002	0.71
Thickness	OP	36	0	0.818
	BW	4	0.081	0.333
	OP × BW	9	0.017	0.529
Opacity	OP	14.12	0.006	0.638
	BW	4.666	0.063	0.368
	OP × BW	37.562	0	0.824

Two-way ANOVA was performed using only T1–T4 in a 2 × 2 factorial design to evaluate the main effects of OP and BW, and their interaction (OP × BW). Each formulation was analysed in triplicate (n = 3). F represents the F-statistic, with 1 and 8 degrees of freedom for the effect and error terms, respectively. Partial η^2 represents the effect size. Effects were considered statistically significant at $p < 0.05$.

The whiteness index (WI) varied among formulations (Table 3), with T5 (without OP) exhibiting the highest value (86.44 ± 0.78) and T6 (without BW) the lowest (50.28 ± 1.66). Among the complete OP–BW formulations, T3 showed the highest WI (70.01 ± 3.34). Two-way ANOVA revealed significant main effects of OP (F = 24.718, $p = 0.001$) and BW (F = 9.894, $p = 0.014$), as well as a significant OP × BW interaction (F = 19.601, $p = 0.002$) (Table 4). These findings indicate that film whiteness depended on both OP and BW concentrations and that the effect of OP varied with BW level. The contrasting WI values of T5 and T6 further suggest that OP contributed substantially to film colour. Such optical characteristics are important for the visual appearance and potential consumer acceptance of edible films [50].

Film thickness varied significantly among formulations, ranging from 0.03 ± 0.01 mm (T6, without BW) to 0.21 ± 0.06 mm (T5, without OP). Among T1–T4, thickness ranged from 0.07 ± 0.01 to 0.09 ± 0.02 mm. Two-way ANOVA revealed significant effects of OP (F = 36.000, $p < 0.001$) and the OP × BW interaction (F = 9.000, $p = 0.017$), whereas BW had no significant main effect ($p = 0.081$; Table 4). Increasing OP level increased thickness at 0.5% BW but had little effect at 1.0% BW, indicating a formulation-dependent interaction. Film opacity ranged from 3.31 ± 0.18 (T5) to 9.27 ± 0.66 (T2), comparable to values reported for orange-peel pectin-based films [51]. The low opacity of T5, together with its high L* and WI, indicated a lighter, more transparent film, whereas OP-containing formulations generally exhibited greater opacity. Two-way ANOVA showed a significant main effect of OP (F = 14.120, $p = 0.006$) and a significant OP × BW interaction (F = 37.562, $p < 0.001$), whereas the main effect of BW was not significant (F = 4.666, $p = 0.063$) (Table 4). Particularly, increasing BW from 0.5% (T2) to 1.0% (T4) at 2.0% OP reduced opacity from 9.27 to 6.52, demonstrating that BW did not consistently increase opacity. Although BW incorporation can enhance light scattering through dispersed lipid domains [52], its effect depends on lipid distribution and interactions within the polymer matrix. Differences in surface roughness and structural heterogeneity may also contribute to film opacity [49], although this was not quantified in the present study.

3.2.2. Film Microstructure

SEM micrographs of the cast films are shown in Figure 4. At ×500 (50 µm scale bar) and ×2000 (10 µm scale bar) magnifications, T1–T3 showed relatively compact and continuous surfaces, with fewer visible pores in T2, whereas T4 showed a heterogeneous surface with numerous cavities, particularly at ×2000. T5 showed surface roughness and localised depressions, and T6 showed the smoothest and most compact surface. These differences may reflect variations in the distribution of OP and BW within the film matrix [53]; however, because only one film per formulation was examined, these observations are descriptive and may not be representative of all films of the same formulation. Moreover, SEM alone cannot confirm lipid aggregation or phase separation [54]. As the films were cast on a flat glass surface under conditions different from those used for fruit coating, their surface morphology may not represent the structure of the coatings formed on the mango peel. An important limitation of this study is that film thickness and SEM morphology were determined on free-standing cast films rather than on the coatings formed on the fruit. Coating deposition on the curved, waxy, and lenticel-bearing mango peel depends on the wettability of the peel, the viscosity of the coating formulation, and drainage and drying conditions and is likely to produce a thinner and less uniform layer than the cast films. The thickness, continuity, and microstructure of the coatings on the fruit were not measured, and the cast-film results should therefore be regarded as indicative of formulation-dependent material properties rather than as direct measurements of the fruit coatings. Future studies should characterise coatings in situ, for example, by gravimetric determination of coating mass per unit surface area, cross-sectional SEM of coated peel, or confocal microscopy using a fluorescent marker.

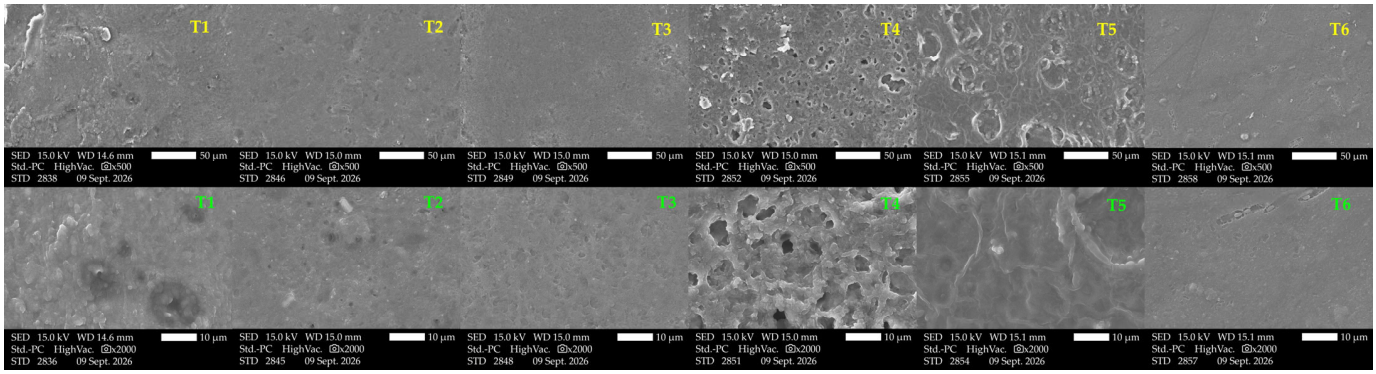


Figure 4. SEM micrographs showing the surface morphology of cast films prepared with different OP and BW formulations (T1–T6). The upper row shows micrographs at ×500 magnification (scale bar = 50 µm), while the lower row shows micrographs at ×2000 magnification (scale bar = 10 µm). Representative micrographs are presented. T1 = 1.0% OP + 0.5% BW, T2 = 2.0% OP + 0.5% BW, T3 = 1.0% OP + 1.0% BW, T4 = 2.0% OP + 1.0% BW, T5 = CTRL-No OP, T6 = CTRL-No BW.

3.3. Implementation of Composite Coatings on Mango Fruit

3.3.1. Surface Frictional Behaviour

The bio-based coating formulations significantly affected both static and kinetic coefficients of friction (COFs) at the mango–corrugated plastic board interface (Figure 5), with values ranging from 0.45 to 0.59 and 0.42 to 0.58, respectively. T4 exhibited the highest static (0.59 ± 0.04) and kinetic COFs (0.58 ± 0.04); however, it differed significantly only from T3 and the uncoated control (T7) and was statistically similar to T1, T2, T5, and T6 (Tukey's HSD, $p > 0.05$). T3 showed the lowest values (0.45 ± 0.01 and 0.42 ± 0.01, respectively), which were significantly lower than those of T1, T2, and T4 for static COF, and of T1, T2, and T4–T6 for kinetic COF. Compared with uncoated fruit (T7; 0.46 ± 0.01 and 0.45 ± 0.01), T3 did not differ significantly in either static or kinetic COF, indicating that coating application did not reduce surface friction relative to uncoated fruit. Two-way ANOVA of T1–T4 (Table 5) revealed significant effects of OP level on static ($F = 19.670$, $p = 0.002$) and kinetic COFs ($F = 29.094$, $p = 0.001$). Significant OP × BW interactions were also observed for static ($F = 14.564$, $p = 0.005$) and kinetic COFs ($F = 17.510$, $p = 0.003$), whereas the main effects of BW were not significant (static $F = 0.521$, $p = 0.491$; kinetic $F = 1.260$, $p = 0.294$). Simple-effects analysis showed that increasing OP from 1.0% to 2.0% increased both COFs at 1.0% BW (T3 vs. T4) but not at 0.5% BW (T1 vs. T2). Conversely, increasing BW from 0.5% to 1.0% reduced static and kinetic COFs at 1.0% OP (T1 vs. T3) but had no significant effect at 2.0% OP (T2 vs. T4; $p = 0.093$ and 0.133). Frictional behaviour therefore depended on the combination of OP and BW levels rather than BW concentration alone. The contrasting COFs of T3 and T4, despite identical BW levels (1.0%), may be associated with differences in coating surface characteristics and interfacial interactions [55]; however, the surface characteristics of the coatings on the fruit were not measured, so this explanation remains a hypothesis. Although the corresponding cast films differed in surface morphology (Figure 4), the coatings on the fruit surface were not examined by SEM, and the mechanisms underlying these frictional differences therefore remain uncertain. Similarly, T6 (without BW) exhibited intermediate COFs that did not differ significantly from those of T1, T2, T4, T5, or T7, further indicating that BW incorporation did not consistently reduce friction [56–58]. As COFs were measured at the mango–corrugated plastic board interface, these findings cannot be directly extrapolated to fruit–fruit contact or transportation conditions. Further studies involving vibration, impact, and bruising assessments are required to establish their implications for mechanical protection during transportation.

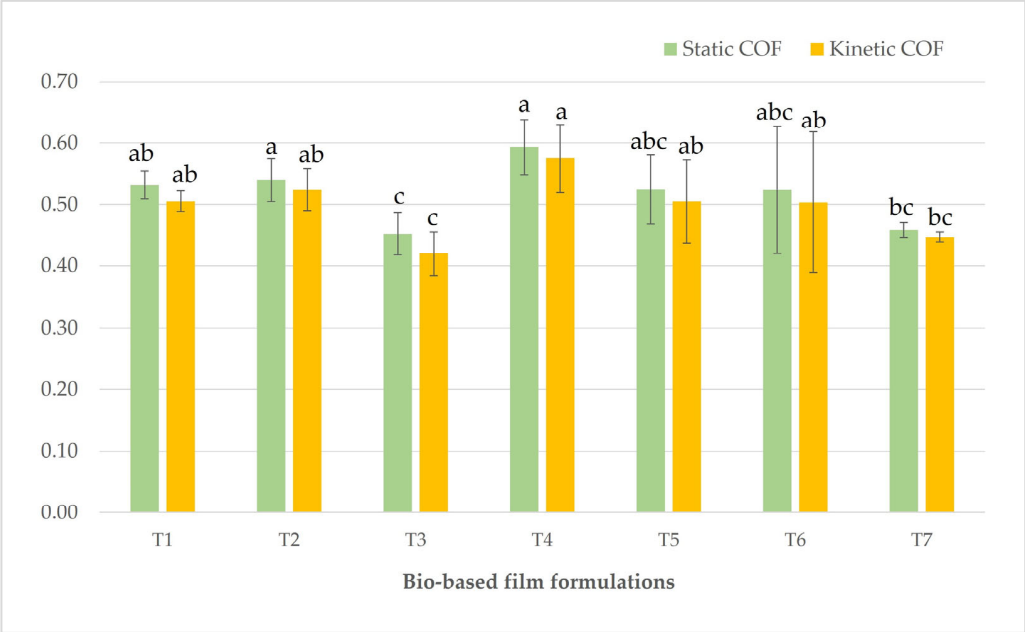


Figure 5. Static and kinetic coefficients of friction (COF) of mangoes treated with coating formulations (T1–T6) and the uncoated control (T7), representing seven treatments in total. Bars represent the mean ± SD of three independent fruit replicates per treatment (n = 3). Different lowercase letters above the bars indicate significant differences among formulations within each COF parameter, as determined by Tukey's HSD test ($p < 0.05$). Statistical comparisons were performed separately for static and kinetic COFs. T1 = 1.0% OP + 0.5% BW; T2 = 2.0% OP + 0.5% BW; T3 = 1.0% OP + 1.0% BW; T4 = 2.0% OP + 1.0% BW; T5 = CTRL–No OP; and T6 = CTRL–No BW.

Table 5. Effects of the main factors (OP and BW) on the static and kinetic coefficients of friction (COFs) of mango fruit coated with bio-based formulations (T1–T4).

Surface Characteristics	Effect	F	*p*-Value	Partial η^2
Static COF	OP	19.67	0.002	0.711
	BW	0.521	0.491	0.061
	OP × BW	14.564	0.005	0.645
Kinetic COF	OP	27.094	0.001	0.772
	BW	1.26	0.294	0.136
	OP × BW	17.51	0.003	0.686

Two-way ANOVA was performed using only T1–T4 in a 2 × 2 factorial design to evaluate the main effects of OP and BW, and their interaction (OP × BW). Each formulation was analysed in triplicate (n = 3). F represents the F-statistic, with 1 and 8 degrees of freedom for the effect and error terms, respectively. Partial η^2 represents the effect size. Effects were considered statistically significant at $p < 0.05$.

3.3.2. Mango Fruit Quality

The bio-based coating formulations significantly affected mango weight loss, firmness, and titratable acidity (TA) after three days of storage, whereas peel L* and a*, total soluble solids (TSS), and pH showed no significant differences among treatments (Table 6). Peel b* showed only a weak overall difference. Weight loss ranged from 3.25 to 4.37%, with T6 (without BW) exhibiting the lowest value (3.25 ± 0.04%), which did not differ significantly from that of T3 (3.45 ± 0.19%). In contrast, T5 (without OP; 4.31 ± 0.03%) and the uncoated control (T7; 4.37 ± 0.19%) showed the highest values, which did not differ significantly from that of T1 (3.92 ± 0.19%). Two-way ANOVA of T1–T4 revealed no significant main effects of OP ($F = 0.237$, $p = 0.640$) or BW ($F = 4.797$, $p = 0.060$) and no significant OP × BW interaction ($F = 4.534$, $p = 0.066$) (Table 7). OP-containing coatings were generally associated with lower

weight loss than the uncoated control, although the effects of OP and BW concentrations within the factorial formulations were not statistically significant. Polysaccharide-based coatings have been reported to reduce moisture loss by forming a semipermeable barrier that limits water transfer and modifies gas exchange [59,60]. However, water-vapour permeability, gas exchange, and the mass and continuity of the coatings on the fruit were not measured in the present study; this mechanism therefore remains a hypothesis. Notably, T6 exhibited the lowest weight loss despite the absence of BW, which suggests, but does not establish, that moisture retention may depend on the OP-based coating matrix and its formulation rather than on the hydrophobic lipid component alone [54].

Table 6. Physicochemical characteristics of mango fruit coated with different coating formulations.

Characteristics	Coating Formulations						No Coating
	T1	T2	T3	T4	T5	T6	T7
Weight loss (%)	3.92 ± 0.19 ^{ab}	3.74 ± 0.27 ^{bc}	3.45 ± 0.19 ^{cd}	3.74 ± 0.02 ^{bc}	4.31 ± 0.03 ^{a}	3.25 ± 0.04 ^{d}	4.37 ± 0.19 ^{a}
Colour							
- L* ^{ns}	61.51 ± 3.50	63.61 ± 2.78	63.08 ± 2.69	60.76 ± 4.24	59.40 ± 6.77	62.23 ± 2.98	58.29 ± 2.30
- a* ^{ns}	9.17 ± 4.14	7.81 ± 2.29	10.84 ± 2.61	9.76 ± 2.15	8.74 ± 3.30	8.02 ± 2.34	7.78 ± 3.13
- b*	55.01 ± 5.58 ^{ab}	53.08 ± 4.05 ^{ab}	53.08 ± 4.01 ^{a}	54.70 ± 3.67 ^{ab}	52.79 ± 4.10 ^{ab}	46.94 ± 8.06 ^{b}	48.79 ± 9.40 ^{ab}
Firmness (g)	187 ± 48 ab	172 ± 30 ^{abc}	169 ± 40 ^{bc}	196 ± 47 ^{ab}	186 ± 40 ^{a}	178 ± 42 ^{bc}	186 ± 54 ^{c}
Total soluble solids (TSS) (°Brix) ^{ns}	13.84 ± 1.37	14.26 ± 1.35	14.28 ± 0.86	14.54 ± 0.63	13.31 ± 1.22	14.10 ± 0.41	13.02 ± 1.05
pH ^{ns}	4.60 ± 0.25	4.71 ± 0.28	4.27 ± 0.21	4.60 ± 0.44	4.61 ± 0.44	4.44 ± 0.21	4.41 ± 0.12
Titratable acidity (TA) (%)	0.44 ± 0.02 ^{a}	0.47 ± 0.01 ^{a}	0.42 ± 0.01 ^{ab}	0.35 ± 0.04 ^{c}	0.37 ± 0.02 ^{bc}	0.24 ± 0.01 ^{d}	0.18 ± 0.02 ^{e}

Values are expressed as mean ± SD (n = 3 independent mango fruits per treatment, representing biological replicates) after 3 days of storage (Day 3). Different superscript letters within the same row indicate significant differences among the seven treatments (T1–T7), as determined by Tukey's HSD test ($p < 0.05$). "ns" indicates no significant difference. T1 = 1.0% OP + 0.5% BW; T2 = 2.0% OP + 0.5% BW; T3 = 1.0% OP + 1.0% BW; T4 = 2.0% OP + 1.0% BW; T5 = CTRL–No OP; and T6 = CTRL–No BW.

Table 7. Effects of the main factors (OP and BW) on physicochemical characteristics of mango fruit coated with bio-based formulations (T1–T4).

Physicochemical Characteristics	Effect	F	*p*-Value	Partial η^2
Weight loss	OP	0.237	0.64	0.029
	BW	4.797	0.06	0.375
	OP × BW	4.534	0.066	0.362
L*	OP	0.004	0.949	0.001
	BW	0.158	0.701	0.019
	OP × BW	1.891	0.206	0.191
a*	OP	1.548	0.249	0.162
	BW	3.425	0.101	0.3
	OP × BW	0.02	0.89	0.003
b*	OP	1.12	0.321	0.123
	BW	0.802	0.397	0.091
	OP × BW	0.003	0.956	0
Firmness	OP	0.216	0.655	0.026
	BW	1.045	0.336	0.116
	OP × BW	8.847	0.018	0.525

Table 7. *Cont.*

Physicochemical Characteristics	Effect	F	*p*-Value	Partial η^2
Total soluble solids (TSS)	OP	0.286	0.608	0.034
	BW	0.32	0.587	0.038
	OP × BW	0.013	0.911	0.002
pH	OP	1.532	0.251	0.161
	BW	1.532	0.251	0.161
	OP × BW	0.36	0.565	0.043
Titratable acidity (TA)	OP	2.178	0.178	0.214
	BW	32.4	0	0.802
	OP × BW	16.044	0.004	0.667

Two-way ANOVA was performed using only T1–T4 in a 2 × 2 factorial design to evaluate the main effects of OP and BW, and their interaction (OP × BW). Each formulation was analysed in triplicate (n = 3). F represents the F-statistic, with 1 and 8 degrees of freedom for the effect and error terms, respectively. Partial η^2 represents the effect size. Effects were considered statistically significant at $p < 0.05$.

Peel L* and a* did not differ significantly among treatments at Day 3 (Table 6). L* ranged from 58.29 ± 2.30 (T7) to 63.61 ± 2.78 (T2), and a* from 7.78 ± 3.13 (T7) to 10.84 ± 2.61 (T3). Peel b* differed among treatments, but only T3 (53.08 ± 4.01) differed significantly from T6 (46.94 ± 8.06), whereas all other treatments were statistically similar. Two-way ANOVA of T1–T4 revealed no significant main effects of OP or BW, or their interaction, on L*, a*, or b* (all $p > 0.10$; Table 7), indicating that variations in OP and BW levels within the investigated ranges did not significantly influence peel colour. Changes in mango peel colour during ripening are associated with chlorophyll degradation and carotenoid development [61], which may be influenced by coating-induced modifications in gas exchange [62]. Similar effects on mango peel colour have been reported for HPMC–beeswax and tragacanth gum coatings [54,62]. However, peel colour was measured only on Day 3, without baseline (Day 0) or time-course measurements, and gas exchange was not measured. These data therefore cannot establish whether the coatings delayed, accelerated, or had no effect on ripening-related colour change.

Fruit firmness differed significantly among treatments at Day 3 (Table 6). T4 showed the highest firmness (196 ± 47 g) and T7 the lowest (172 ± 30 g), whereas T1–T4 and T6 were intermediate. Two-way ANOVA of T1–T4 revealed a significant OP × BW interaction ($F = 8.847$, $p = 0.018$), while the main effects of OP ($F = 0.216$, $p = 0.655$) and BW ($F = 1.045$, $p = 0.336$) were not significant (Table 7). As shown in Table 6, increasing BW level from 0.5% to 1.0% decreased the mean firmness at 1.0% OP (T1 vs. T3: 187 vs. 169 g), whereas firmness increased slightly at 2.0% OP (T2 vs. T4: 172 vs. 196 g). Similarly, increasing OP level from 1.0% to 2.0% decreased firmness at 0.5% BW (T1 vs. T2: 187 vs. 172 g) but increased firmness at 1.0% BW (T3 vs. T4: 169 vs. 196 g). However, these differences should be interpreted cautiously, as the statistical significance of the individual contrasts cannot be established from the reported multiple-comparison groupings alone. Mango softening is associated with enzymatic degradation of cell-wall polysaccharides [63], which may be influenced by coating-induced changes in respiration and ethylene production [64]. However, respiration and ethylene production were not measured, and firmness was determined only on Day 3; the present findings therefore do not establish that the coatings reduced softening or delayed ripening.

TSS and pH did not differ significantly among treatments at Day 3. TSS ranged from 13.02 °Brix (T7) to 14.54 °Brix (T4), while pH ranged from 4.27 (T3) to 4.71 (T2). Two-way ANOVA revealed no significant main effects of OP or BW, or their interaction, on either parameter (all $p > 0.05$; Table 7). The OP × BW interaction was not significant for

TSS (F = 0.013, p = 0.911) or pH (F = 0.360, p = 0.565). Although TSS generally increases during mango ripening through starch hydrolysis and sugar accumulation, polysaccharide-based coatings may influence these processes by modifying respiration and ripening metabolism [65]. Nonetheless, the present results provide no evidence of coating-induced changes in TSS or pH at Day 3, and ripening-related trends cannot be established without baseline and time-course measurements.

TA differed significantly among treatments at Day 3, ranging from 0.18 ± 0.02% in T7 to 0.47 ± 0.01% in T2. T1 (0.44 ± 0.02%) and T2 shared the highest group, and T3 (0.42 ± 0.01%) did not differ from either. The complete OP–BW formulations (T1–T4) generally exhibited higher TA (0.35–0.47%) than the formulation controls (T5 and T6) and uncoated fruit (T7), although T4 (0.35 ± 0.04%) did not differ from T5 (0.37 ± 0.02%). Two-way ANOVA revealed a significant main effect of BW (F = 32.400, p < 0.001) and an OP × BW interaction (F = 16.044, p = 0.004), whereas the OP main effect was not significant (F = 2.178, p = 0.178; Table 7). Simple-effects analysis showed that increasing BW from 0.5% to 1.0% reduced TA significantly at 2.0% OP but not at 1.0% OP (T1 vs. T3). Increasing OP from 1.0% to 2.0% reduced TA at 1.0% BW (T3 vs. T4) but not at 0.5% BW (T1 vs. T2), indicating a formulation-dependent interaction. Organic acids generally decrease during mango ripening as they are utilised in respiration, while edible coatings have been reported to influence acid metabolism by modifying gas exchange [54,66,67]. Interestingly, T6 exhibited the lowest weight loss but relatively low TA, suggesting that the coating characteristics associated with these quality attributes may differ [68]. Variations in OP–BW interactions and coating barrier properties may contribute to these responses [66]. However, gas permeability, respiration rate, and organic acid changes over time were not measured, so these explanations remain hypotheses, and the higher TA observed in coated mangoes cannot be directly attributed to delayed ripening or greater acid retention.

3.3.3. Multivariate Analysis of Composite Coating on Mango Fruit

An exploratory PCA of static COF, kinetic COF, weight loss, and TA is presented in the Supplementary Materials (Figure S1; Table S1). The first two components explained 79.73% of the total variance (PC1: 52.03%, eigenvalue = 2.081; PC2: 27.70%, eigenvalue = 1.108). PC1 was mainly associated with static and kinetic COF (loadings 0.982 and 0.963, respectively; together accounting for 90.9% of the PC1 variance), whereas PC2 was mainly associated with weight loss (loading 0.793), which was contrasted with TA (loading −0.625). Static and kinetic COF were strongly correlated (r = 0.988, p < 0.001), as also reflected by the near-zero eigenvalue of PC4 (0.008); friction therefore contributed two of the four variables and may have disproportionately influenced PC1. When only static COF was included, the first two components explained 74.97% of the total variance (PC1: 45.06%), and the variables contributed more evenly to PC1 (static COF 0.668, weight loss −0.590, TA 0.746). In this reduced analysis, the uncoated control (T7) remained separated from the coated treatments along PC1, whereas T3 no longer separated from the other formulations along PC1 and was positioned close to T6, indicating that the distinct position of T3 in the four-variable PCA was driven largely by friction. Given the small number of variables and fruits, the PCA was used only to visualise relationships among variables and should not be interpreted as a ranking of coating formulations.

4. Conclusions

Okra-processing biomass was valorised as a source of pectin-rich polysaccharides for developing functional bio-based composite coatings for mango fruit. Microwave-assisted extraction provided a numerically, but not significantly, higher yield than conventional thermal extraction and produced OP with comparable methoxyl content and degree of

esterification, although equivalent weight, AUA content, and hydration properties differed between extraction methods. The levels of OP and BW, together with their interactions, influenced the optical properties of cast films and the friction of coated fruit against corrugated plastic board, demonstrating formulation-dependent coating performance. Among the complete OP–BW formulations, T3 (1.0% OP + 1.0% BW) exhibited the lowest static and kinetic coefficients of friction (COFs); however, these values did not differ significantly from those of uncoated fruit. T4 (2.0% OP + 1.0% BW) showed the highest mean values, although it differed significantly only from T3 and the uncoated control. The effect of BW on friction depended on OP concentration, and BW incorporation did not consistently reduce surface friction. After three days of storage, coating treatments significantly affected weight loss, firmness, and TA, with T6 showing the lowest weight loss (3.25%), T4 the highest firmness (196 g), and T1 and T2 the highest TA (0.44–0.47%). However, peel L* and a*, TSS, and pH were unaffected. The preferred COF depends on the packaging system, as lower friction may reduce tangential forces during sliding, whereas higher friction may restrict fruit movement. Thus, formulation selection should consider the intended application and packaging conditions. Okra-derived pectin-rich polysaccharides show potential as sustainable coatings for modifying fruit–packaging friction and selected postharvest quality attributes. Further studies are needed to assess their effectiveness in reducing transportation-induced damage under mango–mango contact, vibration, and impact conditions, while considering bruising and weight loss at different stacking positions.

Supplementary Materials: The following supporting information can be downloaded at https://www.mdpi.com/article/10.3390/polysaccharides7040125/s1, Table S1. Raw data supporting the physicochemical characterisation of okra-derived pectin-rich polysaccharides, bio-based film properties, surface friction measurements, and quality assessments of mango fruit. Figure S1. Exploratory PCA. Table S2. Results of the exploratory principal component analysis (PCA) of static COF, kinetic COF, weight loss, and titratable acidity (TA) of mango fruit (T1–T7; 21 fruits, n = 3 per treatment). Table S3. Statistical analyses using Tukey's HSD (one-way ANOVA). Table S4. Statistical analyses using Tukey's HSD (two-way ANOVA).

Author Contributions: Conceptualisation, P.C. and M.W.; methodology, M.W., P.C. and N.P.; validation, P.C., M.W. and N.P.; formal analysis, T.B., K.T., S.T. and R.J.; investigation, P.C., M.W., N.P., K.T. and S.T.; resources, R.J. and T.B.; data curation, P.C., M.W. and A.I.; writing—original draft preparation, P.C. and M.W.; writing—review and editing, M.W., N.P., B.T. and N.S.; visualisation, P.C., M.W. and A.I.; supervision, M.W. and P.C.; project administration, M.W., B.T. and N.S.; funding acquisition, M.W. All authors have read and agreed to the published version of the manuscript.

Funding: This research was partially supported by the National Research Council of Thailand (NRCT) under Grant No. N23H690018 (2026).

Data Availability Statement: The original contributions presented in this study are included in the article/Supplementary Materials. Further inquiries can be directed to the corresponding author.

Acknowledgments: We would like to express our sincere gratitude to the Interdisciplinary and Technological College, Rajamangala University of Technology Lanna, and the Bioactive Compound Laboratory, Faculty of Agriculture, Chiang Mai University, Chiang Mai, Thailand, for providing the facilities and infrastructure that supported this research.

Conflicts of Interest: The authors declare no conflicts of interest.

References

1. Li, S.; Ren, Y.; Hou, Y.; Zhan, Q.; Jin, P.; Zheng, Y.; Wu, Z. Polysaccharide-Based Composite Films: Promising Biodegradable Food Packaging Materials. *Foods* **2024**, *13*, 3674. [CrossRef] [PubMed]
2. Costa, D.L.M.G.d. Produção por Extrusão de Filmes de Alto Teor de Amido Termoplástico com Poli (Butileno Adipato Co-Tereftalato) (PBAT). Master's Thesis, Universidade Estadual de Londrina, Londrina, Brazil, 2024.

3. Syarifuddin, A.; Muflih, M.H.; Izzah, N.; Fadillah, U.; Ainani, A.F.; Dirpan, A. Pectin-based edible films and coatings: From extraction to application on food packaging towards circular economy—A review. *Carbohydr. Polym. Technol. Appl.* **2025**, *9*, 100680. [CrossRef]
4. Eshetu, A.; Ibrahim, A.M.; Forsido, S.F.; Kuyu, C.G. Effect of beeswax and chitosan treatments on quality and shelf life of selected mango (*Mangifera indica* L.) cultivars. *Heliyon* **2019**, *5*, e01116. [CrossRef] [PubMed]
5. Amin, U.; Khan, M.K.I.; Khan, M.U.; Ehtasham Akram, M.; Pateiro, M.; Lorenzo, J.M.; Maan, A.A. Improvement of the performance of chitosan—Aloe vera coatings by adding beeswax on postharvest quality of mango fruit. *Foods* **2021**, *10*, 2240. [CrossRef] [PubMed]
6. Sengkhamparn, N.; Sagis, L.M.; De Vries, R.; Schols, H.A.; Sajjaanantakul, T.; Voragen, A.G. Physicochemical properties of pectins from okra (*Abelmoschus esculentus* (L.) Moench). *Food Hydrocoll.* **2010**, *24*, 35–41. [CrossRef]
7. Sengkhamparn, N.; Verhoef, R.; Schols, H.A.; Sajjaanantakul, T.; Voragen, A.G. Characterisation of cell wall polysaccharides from okra (*Abelmoschus esculentus* (L.) Moench). *Carbohydr. Res.* **2009**, *344*, 1824–1832. [CrossRef] [PubMed]
8. Dantas, T.L.; Alonso Buriti, F.C.; Florentino, E.R. Okra (*Abelmoschus esculentus* L.) as a potential functional food source of mucilage and bioactive compounds with technological applications and health benefits. *Plants* **2021**, *10*, 1683. [CrossRef] [PubMed]
9. Zhu, X.-M.; Xu, R.; Wang, H.; Chen, J.-Y.; Tu, Z.-C. Structural properties, bioactivities, and applications of polysaccharides from Okra [*Abelmoschus esculentus* (L.) Moench]: A review. *J. Agric. Food Chem.* **2020**, *68*, 14091–14103. [CrossRef] [PubMed]
10. Araújo, A.; Galvão, A.; Silva Filho, C.; Mendes, F.; Oliveira, M.; Barbosa, F.; Sousa Filho, M.; Bastos, M. Okra mucilage and corn starch bio-based film to be applied in food. *Polym. Test.* **2018**, *71*, 352–361. [CrossRef]
11. Olawuyi, I.F.; Lee, W.Y. Development and characterization of biocomposite films based on polysaccharides derived from okra plant waste for food packaging application. *Polymers* **2022**, *14*, 4884. [CrossRef] [PubMed]
12. Wongkaew, M.; Kittiwachana, S.; Phuangsaijai, N.; Tinpovong, B.; Tiyayon, C.; Pusadee, T.; Chuttong, B.; Sringarm, K.; Bhat, F.M.; Sommano, S.R. Fruit characteristics, peel nutritional compositions, and their relationships with mango peel pectin quality. *Plants* **2021**, *10*, 1148. [CrossRef] [PubMed]
13. Wongkaew, M.; Sommano, S.R.; Tangpao, T.; Rachtanapun, P.; Jantanasakulwong, K. Mango Peel Pectin by Microwave-Assisted Extraction and Its Use as Fat Replacement in Dried Chinese Sausage. *Foods* **2020**, *9*, 450. [CrossRef] [PubMed]
14. Guandalini, B.B.V.; Rodrigues, N.P.; Marczak, L.D.F. Sequential extraction of phenolics and pectin from mango peel assisted by ultrasound. *Food Res. Int.* **2019**, *119*, 455–461. [CrossRef] [PubMed]
15. Girma, E.; Worku, T. Extraction and characterization of pectin from selected fruit peel waste. *Int. J. Sci. Res. Publ.* **2016**, *6*, 447–454. [CrossRef]
16. Virk, B.; Sogi, D. Extraction and characterization of pectin from apple (*Malus pumila*. Cv Amri) peel waste. *Int. J. Food Prop.* **2004**, *7*, 693–703. [CrossRef]
17. Wang, F.; Du, C.; Chen, J.; Shi, L.; Li, H. A new method for determination of pectin content using spectrophotometry. *Polymers* **2021**, *13*, 2847. [CrossRef] [PubMed]
18. Beuchat, L.R. Functional and electrophoretic characteristics of succinylated peanut flour protein. *J. Agric. Food Chem.* **1977**, *25*, 258–261. [CrossRef]
19. Kaur, M.; Singh, N. Studies on functional, thermal and pasting properties of flours from different chickpea (*Cicer arietinum* L.) cultivars. *Food Chem.* **2005**, *91*, 403–411. [CrossRef]
20. Chaichi, M.; Hashemi, M.; Badii, F.; Mohammadi, A. Preparation and characterization of a novel bionanocomposite edible film based on pectin and crystalline nanocellulose. *Carbohydr. Polym.* **2017**, *157*, 167–175. [CrossRef] [PubMed]
21. Chao, Z.; Yue, M.; Xiaoyan, Z.; Dan, M. Development of soybean protein-isolate edible films incorporated with beeswax, Span 20, and glycerol. *J. Food Sci.* **2010**, *75*, C493–C497. [CrossRef] [PubMed]
22. Wang, H.; Liao, Y.; Zhu, G.; Wang, L.; Chen, Z.; Li, X.; Wang, C.; Yu, J.; Song, P. Development of Double-Film Composite Food Packaging with UV Protection and Microbial Protection for Cherry Preservation. *Foods* **2025**, *14*, 2283. [CrossRef] [PubMed]
23. Liu, J.; Liu, S.; Chen, Y.; Zhang, L.; Kan, J.; Jin, C. Physical, mechanical and antioxidant properties of chitosan films grafted with different hydroxybenzoic acids. *Food Hydrocoll.* **2017**, *71*, 176–186. [CrossRef]
24. Sandi, O.M.; Muhandri, T.; Suyatma, N.E. Optimasi Pembuatan Heat Sealable Film dari Kolang-Kaling sebagai Bahan Kemasan. *J. Teknol. Dan Ind. Pangan* **2024**, *35*, 79–91. [CrossRef]
25. Kelemenová, T.; Dovica, M.; Božek, P.; Koláriková, I.; Benedik, O.; Virgala, I.; Prada, E.; Miková, Ľ.; Kot, T.; Kelemen, M. Specific Problems in Measurement of Coefficient of Friction Using Variable Incidence Tribometer. *Symmetry* **2020**, *12*, 1235. [CrossRef]
26. Xu, B.; Wu, S. Preservation of mango fruit quality using fucoidan coatings. *LWT* **2021**, *143*, 111150. [CrossRef]
27. Truc, N.T.; Uthairatanakij, A.; Srilaong, V.; Laohakunjit, N.; Jitareerat, P. Effect of electron beam radiation on disease resistance and quality of harvested mangoes. *Radiat. Phys. Chem.* **2021**, *180*, 109289. [CrossRef]
28. Yang, W.; Chen, Y.; Li, K.; Jin, W.; Zhang, Y.; Liu, Y.; Ren, Z.; Li, Y.; Chen, P. Optimization of microwave-expanding pretreatment and microwave-assisted extraction of hemicellulose from bagasse cells with the exploration of the extracting mechanism. *Carbohydr. Polym.* **2024**, *330*, 121814. [CrossRef] [PubMed]

29. Tran, C.H.; Vu, T.T.H.; Le, N.H.; Phan, V.M. Microwave-Assisted Extraction of Polysaccharides From the Abelmoschus sagittifolius: Optimization, Structure, and Bioactivity. *J. Food Process. Preserv.* **2024**, *2024*, 8862451. [CrossRef]
30. Fatima, M.; Rakha, A.; Saeed, M.; Shahid, M.; Van Bockstaele, F. Okra varieties: Effect of different extraction techniques on the physicochemical, functional, and morphological attributes of okra polysaccharides. *J. Food Meas. Charact.* **2025**, *19*, 549–564. [CrossRef]
31. Alkanan, Z.T.; Altemimi, A.B.; Hassan, N.A.; Didar, Z.; Hesarinejad, M.A.; Rahman Salama, N.A.; Al-Hashimi, A.G.; Cacciola, F.; Abedelmaksoud, T.G. Effects of Microwave Utilization on the Color Properties of Food: A Review. *ChemBioEng Rev.* **2024**, *11*, 483–494. [CrossRef]
32. Lund, M.N.; Ray, C.A. Control of Maillard Reactions in Foods: Strategies and Chemical Mechanisms. *J. Agric. Food Chem.* **2017**, *65*, 4537–4552. [CrossRef] [PubMed]
33. Tapia, M.S.; Alzamora, S.M.; Chirife, J. Effects of Water Activity (a_w) on Microbial Stability as a Hurdle in Food Preservation. In *Water Activity in Foods*; Wiley: Hoboken, NJ, USA, 2020; pp. 323–355.
34. Beuchat, L.R. Influence of Water Activity on Growth, Metabolic Activities and Survival of Yeasts and Molds. *J. Food Prot.* **1983**, *46*, 135–141. [CrossRef] [PubMed]
35. Cebeci Aydın, F.; Erten, T. Microwave-Assisted Extraction of Pectin from Pickled Cabbage Waste: Process Optimisation, Characterisation and Application in Low-Sugar Jam. *Polymers* **2026**, *18*, 2200. [CrossRef] [PubMed]
36. Forouhar, A.; Hamdami, N.; Djelveh, G.; Gardarin, C.; Pierre, G.; Ursu, A.V.; Michaud, P. The Effect of Ultrasound Pretreatment on Pectin Extraction from Watermelon Rind Using Microwave-Assisted Extraction. *Appl. Sci.* **2023**, *13*, 5558. [CrossRef]
37. Ritzoulis, C. Mucilage formation in food: A review on the example of okra. *Int. J. Food Sci. Technol.* **2017**, *52*, 59–67. [CrossRef]
38. Miganeh Waiss, I.; Kimbonguila, A.; Mohamed Abdoul-Latif, F.; Nkeletela, L.B.; Scher, J.; Petit, J.R.M. Total phenolic content, antioxidant activity, shelf-life and reconstitutability of okra seeds powder: Influence of milling and sieving processes. *Int. J. Food Sci. Technol.* **2021**, *56*, 5139–5149. [CrossRef]
39. Deli, M.; Petit, J.; Nguimbou, R.M.; Beaudelaire Djantou, E.; Njintang Yanou, N.; Scher, J. Effect of sieved fractionation on the physical, flow and hydration properties of *Boscia senegalensis* Lam., *Dichostachys glomerata* Forssk. and *Hibiscus sabdariffa* L. powders. *Food Sci. Biotechnol.* **2019**, *28*, 1375–1389. [CrossRef] [PubMed]
40. Einhorn-Stoll, U. Pectin-water interactions in foods—From powder to gel. *Food Hydrocoll.* **2018**, *78*, 109–119. [CrossRef]
41. Xiang, T.; Yang, R.; Li, L.; Lin, H.; Kai, G. Research progress and application of pectin: A review. *J. Food Sci.* **2024**, *89*, 6985–7007. [CrossRef] [PubMed]
42. Said, N.S.; Olawuyi, I.F.; Lee, W.Y. Pectin Hydrogels: Gel-Forming Behaviors, Mechanisms, and Food Applications. *Gels* **2023**, *9*, 732. [CrossRef] [PubMed]
43. Dranca, F.; Oroian, M. Extraction, purification and characterization of pectin from alternative sources with potential technological applications. *Food Res. Int.* **2018**, *113*, 327–350. [CrossRef] [PubMed]
44. Saravanan, R.; Jeevitha, G.C. Sustainable Approach for Utilization of Mango Peel Wastes for Pectin Extraction by Natural Deep Eutectic Solvents. *J. Food Process. Preserv.* **2024**, *2024*, 4540390. [CrossRef]
45. Gnanasambandam, R.; Proctor, A. Determination of pectin degree of esterification by diffuse reflectance Fourier transform infrared spectroscopy. *Food Chem.* **2000**, *68*, 327–332. [CrossRef]
46. Devkota, K. Beekeeping: Sustainable Livelihoods and Agriculture Production in Nepal. In *Modern Beekeeping—Bases for Sustainable Production*; Rebolledo Ranz, R.E., Ed.; IntechOpen: London, UK, 2020.
47. Wilson, R.H.; Smith, A.C.; Kacuráková, M.; Saunders, P.K.; Wellner, N.; Waldron, K.W. The mechanical properties and molecular dynamics of plant cell wall polysaccharides studied by Fourier-transform infrared spectroscopy. *Plant Physiol.* **2000**, *124*, 397–405. [CrossRef] [PubMed]
48. Coimbra, M.A.; Barros, A.; Barros, M.; Rutledge, D.N.; Delgadillo, I. Multivariate analysis of uronic acid and neutral sugars in whole pectic samples by FT-IR spectroscopy. *Carbohydr. Polym.* **1998**, *37*, 241–248. [CrossRef]
49. Abdellatif, H.R.S.; Helmy, M.M.; Younis, H.G.R. Synthesis and characterization of edible films using high methoxyl pectin extracted from orange peel. *Sci. Rep.* **2026**, *16*, 11364. [CrossRef] [PubMed]
50. Sarafidou, M.; Tsouko, E.; Giannoulis, A.; Briassoulis, D.; Baltatzis, G.E.; Trougakos, I.P.; Tsironi, T.; Koutinas, A. Engineering Pectin Biobased Films with Bacterial Cellulose Nanostructures for Enhanced Food Packaging Performance. *ACS Food Sci. Technol.* **2025**, *5*, 3374–3386. [CrossRef] [PubMed]
51. Castillo-Rodríguez, L.; Hernández-Cázares, A.-S.; Rojas-López, M.; Hidalgo-Contreras, J.-V.; López-Malo, A.; Rios-Corripio, M.-A. Development of edible films based on pectin and essential oil extracted from orange (*Citrus sinensis*) peel using a central composite design. *CyTA-J. Food* **2025**, *23*, 2525175. [CrossRef]
52. Maftoonazad, N.; Ramaswamy, H.S.; Marcotte, M. Evaluation of Factors Affecting Barrier, Mechanical and Optical Properties of Pectin-Based Films Using Response Surface Methodology. *J. Food Process Eng.* **2007**, *30*, 539–563. [CrossRef]

53. Esfandiari, Z.; Hassani, B.; Sani, I.K.; Talebi, A.; Mohammadi, F.; Zomorodi, S.; Kaveh, M.; Assadpour, E.; Khodaei, S.M.; Eghbaljoo, H.; et al. Characterization of edible films made with plant carbohydrates for food packaging: A comprehensive review. *Carbohydr. Polym. Technol. Appl.* **2025**, *11*, 100979. [CrossRef]
54. Sousa, F.F.; Pinsetta Junior, J.S.; Oliveira, K.; Rodrigues, E.C.N.; Andrade, J.P.; Mattiuz, B.H. Conservation of 'Palmer' mango with an edible coating of hydroxypropyl methylcellulose and beeswax. *Food Chem.* **2021**, *346*, 128925. [CrossRef] [PubMed]
55. Fabra, M.J.; Talens, P.; Chiralt, A. Microstructure and optical properties of sodium caseinate films containing oleic acid–beeswax mixtures. *Food Hydrocoll.* **2009**, *23*, 676–683. [CrossRef]
56. Liu, R.; Zhang, R.; Zhai, X.; Li, C.; Hou, H.; Wang, W. Effects of beeswax emulsified by octenyl succinate starch on the structure and physicochemical properties of acid-modified starchfilms. *Int. J. Biol. Macromol.* **2022**, *219*, 262–272. [CrossRef] [PubMed]
57. Han, J.H.; Seo, G.H.; Park, I.M.; Kim, G.N.; Lee, D.S. Physical and Mechanical Properties of Pea Starch Edible Films Containing Beeswax Emulsions. *J. Food Sci.* **2006**, *71*, E290–E296. [CrossRef]
58. Yang, L.; Paulson, A.T. Effects of lipids on mechanical and moisture barrier properties of edible gellan film. *Food Res. Int.* **2000**, *33*, 571–578. [CrossRef]
59. Wu, J.; Zhang, L.; Fan, K. Recent advances in polysaccharide-based edible coatings for preservation of fruits and vegetables: A review. *Crit. Rev. Food Sci. Nutr.* **2024**, *64*, 3823–3838. [CrossRef] [PubMed]
60. Tavassoli-Kafrani, E.; Gamage, M.V.; Dumée, L.F.; Kong, L.; Zhao, S. Edible films and coatings for shelf life extension of mango: A review. *Crit. Rev. Food Sci. Nutr.* **2022**, *62*, 2432–2459. [CrossRef] [PubMed]
61. Ketsa, S.; Phakawatmongkol, W.; Subhadrabhandhu, S. Peel Enzymatic Activity and Colour Changes in Ripening Mango Fruit. *J. Plant Physiol.* **1999**, *154*, 363–366. [CrossRef]
62. Ali, S.; Zahid, N.; Nawaz, A.; Naz, S.; Ejaz, S.; Ullah, S.; Siddiq, B. Tragacanth gum coating suppresses the disassembly of cell wall polysaccharides and delays softening of harvested mango (*Mangifera indica* L.) fruit. *Int. J. Biol. Macromol.* **2022**, *222*, 521–532. [CrossRef] [PubMed]
63. Yashoda, H.M.; Prabha, T.N.; Tharanathan, R.N. Mango ripening: Changes in cell wall constituents in relation to textural softening. *J. Sci. Food Agric.* **2006**, *86*, 713–721. [CrossRef]
64. Ali, S.; Ishtiaq, S.; Nawaz, A.; Naz, S.; Ejaz, S.; Haider, M.W.; Shah, A.A.; Ali, M.M.; Javad, S. Layer by layer application of chitosan and carboxymethyl cellulose coatings delays ripening of mango fruit by suppressing cell wall polysaccharides disassembly. *Int. J. Biol. Macromol.* **2024**, *256*, 128429. [CrossRef] [PubMed]
65. Cosme Silva, G.M.; Silva, W.B.; Medeiros, D.B.; Salvador, A.R.; Cordeiro, M.H.M.; da Silva, N.M.; Santana, D.B.; Mizobutsi, G.P. The chitosan affects severely the carbon metabolism in mango (*Mangifera indica* L. cv. Palmer) fruit during storage. *Food Chem.* **2017**, *237*, 372–378. [CrossRef] [PubMed]
66. Wei, S.; Mei, J.; Xie, J. Effects of Edible Coating and Modified Atmosphere Technology on the Physiology and Quality of Mangoes after Low-Temperature Transportation at 13 °C in Vibration Mitigation Packaging. *Plants* **2021**, *10*, 2432. [CrossRef] [PubMed]
67. Yin, C.; Huang, C.; Wang, J.; Liu, Y.; Lu, P.; Huang, L. Effect of Chitosan- and Alginate-Based Coatings Enriched with Cinnamon Essential Oil Microcapsules to Improve the Postharvest Quality of Mangoes. *Materials* **2019**, *12*, 2039. [CrossRef] [PubMed]
68. Baldwin, E.A.; Burns, J.K.; Kazokas, W.; Brecht, J.K.; Hagenmaier, R.D.; Bender, R.J.; Pesis, E. Effect of two edible coatings with different permeability characteristics on mango (*Mangifera indica* L.) ripening during storage. *Postharvest Biol. Technol.* **1999**, *17*, 215–226. [CrossRef]

Disclaimer/Publisher's Note: The statements, opinions and data contained in all publications are solely those of the individual author(s) and contributor(s) and not of MDPI and/or the editor(s). MDPI and/or the editor(s) disclaim responsibility for any injury to people or property resulting from any ideas, methods, instructions or products referred to in the content.